Form Optimization Control for Multiple Objects Transportation by Transformable Multirotor with Two-dimensional Multilinks

Tomoki Anzai[1], Moju Zhao[1], Xiangyu Chen[1], Fan Shi[1], Koji Kawasaki[1], Kei Okada[1], Masayuki Inaba[1]

Abstract— In this paper, zoi

I. INTRODUCTION

Recently, aerial robots have attracted a lot of attention and have been studied actively due to their high mobility in three-dimentional environments[1]. Moreover, as a way to take this advantage, object transportation by aerial robot has become an active area of research. For instance, Lindsey et al.[2] proposed a system in which teams of quadrotor helicopters assemble 2.5-D structures. However, there are still some problems to solve on aerial object transportation. In particular, the endurance of aerial robot is a significant problem. To make the endurance longer, putting bigger battries can be considered as a way, but the endurance does not scale linearly with the batteries capacity due to their large weight. Moreover, large weight causes unstability of flight. Therefore, it is not easy to make the endurance longer, so we must change the point of view.

To improve the efficiency of aerial object transportation within the limited endurance, we focus on a way that aerial robot transports multiple objects at the same time. However, it is difficult for conventional aerial robots to transport multiple objects because multiple grippers are necessary to grasp multiple objects, but when the number of objects the aerial robot grasps changes, the position of center of gravity(CoG) of the aerial robot changes, and the flight control becomes unstable. Therefore, to achieve this purpose, we focus on multirotor with two-dimensional multilinks[3] which has the ability to modify the position of CoG actively. When picking up an object, the multirotor with multilinks can keep the flight control stable by the aerial transformation by which the position of CoG can be modified.

The main purpose of this paper is to achieve the multiple objects transportation by the multirotor with multilinks, along with the configuration of hardware and software system. Sec. II describes the general approach for the multiple objects transportation. Sec. III clarifies the model of

[1]T. Anzai, M. Zhao, X. Chen, F. Shi, K. Kawasaki, K. Okada and M. Inaba are with Department of Mechano-Informatics, The University of Tokyo, 7-3-1 Hongo, Bunkyo-Ku, Tokyo 113-8656, Japan `anzai at jsk.t.u-tokyo.ac.jp`
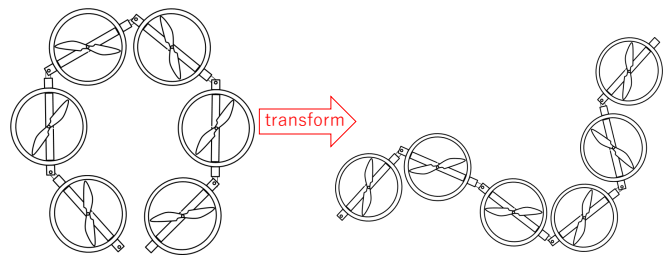
Fig. 1.   multiple object transportation.

Fig. 2.   multi link.

the transformable aerial robot and flight control for aerial transformation. Sec. IV explains how to find the optimal form of the multirotor with multilinks based on the flight stability. In Sec. V, the hardware and software system of the multirotor with multilinks are revealed. Finally, we present experimental results in Sec. VI to demonstrate the feasibility of the multiple object transportation by the multirotor with multilinks.

II. APPROACHES TO MULTIPLE OBJECT TRANSPORTATION

A. Transformable Multirotor with Two-dimensional Multi-links

Zhao et al.[3] proposed a transformable multirotor comprising link modules with built-in propellers and achieved the stable aerial transformation. In another work[4], they achieved the aerial manipulation by using the whole body of the transformable aerial robot. The joints with the same rotational axis allows the two-dimensional transformation as shown in Fig. 2. In this work, we focus on the fact that this aerial robot has the ability to modify the position of CoG actively. Thus, this aerial robot can keep the flight stable by aerial transformation although the number of objects it grasps changes. Therefore, using this way, we approach to the multiple object transportation.

B. Form Optimization Based on Flight Stability

To keep the flight stable by aerial transformation, the multirotor with multilinks must transform to a particular form. In this work, to obtain the form, we propose the method of form optimization based on flight stability. In Sec. IV, firstly, we investigate the definition of flight stability. Secondly, constraints of form considering the geometric condition and control stability is introduced. Finally, optimal form is obtained by using gradient descent.

C. Hardware and Software System

To transport objects by aerial robots, grippers are necessary for grasp objects. Hense, we develop an electromagnet gripper and whole hardware and software system including the link module of multilink and the multi-layer structure for internal communication. In Sec. V, we explain the system in detail.

III. FLIGHT CONTROL FOR AERIAL TRANSFORMATION

A. Dynamic Model

We assume that the multilinks act as a single rigid body at each time point, since the aerial transformation is operated slowly. With this assumption, the dynamics of the translational motion and rotational motion can be written as follows:

$$M\ddot{\boldsymbol{r}}_{CoG} = \begin{bmatrix} 0 \\ 0 \\ -Mg \end{bmatrix} + R \begin{bmatrix} 0 \\ 0 \\ \sum_{i=1}^{N} F_i \end{bmatrix}; R = R_z(\psi)R_y(\theta)R_x(\varphi) \tag{1}$$

$$I_{multilink}\begin{bmatrix} \dot{w_x} \\ \dot{w_y} \\ \dot{w_z} \end{bmatrix} = \begin{bmatrix} \sum_{i=1}^{N} y_iF_i \\ -\sum_{i=1}^{N} x_iF_i \\ \sum_{i=1}^{N} T_i \end{bmatrix} - \begin{bmatrix} w_x \\ w_y \\ w_z \end{bmatrix} \times I_{multilink}\begin{bmatrix} w_x \\ w_y \\ w_z \end{bmatrix} \tag{2}$$

where $\boldsymbol{r}_{CoG}$ and $I_{multilink}$ are the positions of the center of mass and the principal moment of inertia respectively. $[\begin{array}{ccc} w_x & w_y & w_z \end{array}]^{\mathrm{T}}$ is the vector of the angular velocity of the multilink ,while $[\begin{array}{ccc} \dot{\varphi} & \dot{\theta} & \dot{\psi} \end{array}]^{\mathrm{T}}$ are the time derivatives of Euler angles roll, pitch and yaw respectively.

B. Attitude and Altitude Control Based on LQI Control

As described in previous work[3], the dynamics of the model can be integrated into the simultaneous equations as follows:

$$\ddot{\boldsymbol{y}} = P\boldsymbol{u} - \boldsymbol{G} \tag{3}$$

$\boldsymbol{y} = [\begin{array}{cccc} z & \varphi & \theta & \psi \end{array}]^{\mathrm{T}}; \ \boldsymbol{u} = [\begin{array}{ccc} F_1 & \cdots & F_N \end{array}]^{\mathrm{T}}; \ \boldsymbol{G} = [\begin{array}{cccc} g & 0 & 0 & 0 \end{array}]^{\mathrm{T}}$

Note that matrix P represents the configuration of the multilinks, including the arrangement of the propellers. It is significant that matrix P is not constant for the transformable multirotor while that is constant for conventional aerial robots.

$$P = [\begin{array}{cccc} \mathbf{p}_z & \mathbf{p}_x & \mathbf{p}_y & \mathbf{p}_c \end{array}]^{\mathrm{T}} \tag{4}$$

$\mathbf{p}_z = [\begin{array}{ccc} \bar{m}_1 & \cdots & \bar{m}_N \end{array}]^{\mathrm{T}}; \ \mathbf{p}_x = [\begin{array}{ccc} \bar{x}_1 & \cdots & \bar{x}_N \end{array}]^{\mathrm{T}};$

$\mathbf{p}_y = [\begin{array}{ccc} \bar{y}_1 & \cdots & \bar{y}_N \end{array}]^{\mathrm{T}}; \ \mathbf{p}_c = [\begin{array}{ccc} \bar{c}_1 & \cdots & \bar{c}_N \end{array}]^{\mathrm{T}};$

$$\bar{x}_i = \frac{-x_i}{I_{multi_{yy}}}, \ \bar{y}_i = \frac{y_i}{I_{multi_{xx}}}, \ \bar{c}_i = \frac{c_i}{I_{multi_{zz}}}, \ \bar{m}_i = \frac{1}{M}$$

We introduce the following state equation for linear-quadratic-integral(LQI) system about attitude and altitude control with the new state($\boldsymbol{x} = [\begin{array}{cccccccc} z & \dot{z} & \varphi & \dot{\varphi} & \theta & \dot{\theta} & \psi & \dot{\psi} \end{array}]^{\mathrm{T}}$).

$$\dot{\boldsymbol{x}} = A\boldsymbol{x} + B\boldsymbol{u} + \boldsymbol{d} \tag{5}$$

$$\boldsymbol{y} = C\boldsymbol{x} \tag{6}$$

$$\boldsymbol{x} \in R^8, \ \boldsymbol{u} \in R^N, \ \boldsymbol{y} \in R^4, \ \boldsymbol{d} \in R^8$$

where

$$A = \begin{bmatrix} 0 & 1 & 0 & 0 & 0 & 0 & 0 & 0 \\ 0 & 0 & 0 & 0 & 0 & 0 & 0 & 0 \\ 0 & 0 & 0 & 1 & 0 & 0 & 0 & 0 \\ 0 & 0 & 0 & 0 & 0 & 0 & 0 & 0 \\ 0 & 0 & 0 & 0 & 0 & 1 & 0 & 0 \\ 0 & 0 & 0 & 0 & 0 & 0 & 0 & 0 \\ 0 & 0 & 0 & 0 & 0 & 0 & 0 & 1 \\ 0 & 0 & 0 & 0 & 0 & 0 & 0 & 0 \end{bmatrix}$$

$$B = [\begin{array}{cccccccc} \mathbf{0} & \boldsymbol{p}_z & \mathbf{0} & \boldsymbol{p}_x & \mathbf{0} & \boldsymbol{p}_y & \mathbf{0} & \boldsymbol{p}_c \end{array}]^{\mathrm{T}}$$

$$C = \begin{bmatrix} 1 & 0 & 0 & 0 & 0 & 0 & 0 & 0 \\ 0 & 0 & 1 & 0 & 0 & 0 & 0 & 0 \\ 0 & 0 & 0 & 0 & 1 & 0 & 0 & 0 \\ 0 & 0 & 0 & 0 & 0 & 0 & 1 & 0 \end{bmatrix}$$

In Eq. 5 $\sim$ Eq. 6, $\boldsymbol{u}$ and $\boldsymbol{y}$ are the input and output of the control system, while $\boldsymbol{d} = [\begin{array}{cccccccc} 0 & -g & 0 & 0 & 0 & 0 & 0 & 0 \end{array}]^{\mathrm{T}}$ can be regarded as constant noise in the control system.

We extend the state equation by modifying the state and input as follows:

$$\tilde{\boldsymbol{x}} \equiv \boldsymbol{x} - \boldsymbol{x}_s; \ \tilde{\boldsymbol{u}} \equiv \boldsymbol{u} - \boldsymbol{u}_s \tag{7}$$

where $\boldsymbol{x}_s$ and $\boldsymbol{u}_s$ are the final values at the steady state.

We also introduce a tracking error between the reference input and the system output e and the integral value v as follows:

$$\dot{v} = e = \boldsymbol{r} - \boldsymbol{y} = C\boldsymbol{x_s} - C\boldsymbol{x} = -C\tilde{\boldsymbol{x}} \tag{8}$$

Based on the extended state equation(Eq. 9), we design a cost function given by Eq. Eq. 10.

$$\dot{\bar{\boldsymbol{x}}} = \bar{A}\bar{\boldsymbol{x}} + \bar{B}\tilde{\boldsymbol{u}} \tag{9}$$

$$\bar{\boldsymbol{x}} = \begin{bmatrix} \tilde{\boldsymbol{x}} \\ \boldsymbol{v} \end{bmatrix}; \ \bar{A} = \begin{bmatrix} A & O_{8,4} \\ -C & O_{4,4} \end{bmatrix}; \ \bar{B} = \begin{bmatrix} B \\ O_{4,N} \end{bmatrix}$$

$$J = \int_0^\infty (\bar{\boldsymbol{x}}^{\mathrm{T}}Q\bar{\boldsymbol{x}} + \tilde{\boldsymbol{u}}^{\mathrm{T}}R\tilde{\boldsymbol{u}})dt \tag{10}$$

where Q and R are the gain matrices to determine the influence on the convergence characteristics of the control system.

Finally we can retrieve the optimal feedback gain from Eq. Eq. 9 and Eq. Eq. 10 arrcoding to the general LQ theory[5].

C. Position Control in the Horizontal Plane

positions control in the x and y planes use the roll and pitch angles as inputs, and the translational accelerations $\ddot{x}$ and $\ddot{y}$ are a consequence of pitch θ and roll φ tilt. The desired accelerations $\ddot{x}^{des}$ and $\ddot{y}^{des}$ are calculated from a general PID controller described in previous work[6]:

$$\ddot{r}_{CoG}^{des} = k_P(r_{CoG}^{des} - r_{CoG}) + k_I \int (r_{CoG}^{des} - r_{CoG})d\tau + k_D(\dot{r}_{CoG}^{des} - \dot{r}_{CoG}) \tag{11}$$

where the PID gains(k_P, k_I, k_D) are adjusted to achieve the stable hovering position control.

IV. FORM OPTIMIZATION BASED ON FLIGHT STABILITY

A. Optimal Form Based on Flight Stability

The dynamics of the model is described is Eq. 4. Therefore, when the control system is at steady state, the control model can be written as follows:

$$P(\boldsymbol{\theta})\boldsymbol{u} = \boldsymbol{G} \tag{12}$$

When any element in $\boldsymbol{u}$ exceeds the range of lifting forces, the flight control is unstable. Although all elements of $\boldsymbol{u}$ fall within the range of forces, any one of them can exceed the range of forces due to flight control when it is close to the upper limit of forces. Hence, the most stable state is that all elements of $\boldsymbol{u}$ are equal since the sum of $\boldsymbol{u}$ equal to MG which is constant at the steady state. This is written as:

$$\min V(\boldsymbol{u}) \text{ subject to } P(\boldsymbol{\theta})\boldsymbol{u} = \boldsymbol{G} \tag{13}$$

where the function $V(x)$ is used to calculate the variance of elements of x.

This variance can be written as:

$$V(\boldsymbol{u}) = E(\boldsymbol{u}^2) - E(\boldsymbol{u})^2 \tag{14}$$

where the function $E(x)$ is used to calculate the mean of elements of x.

Note that $E(\boldsymbol{u})^2$ is a constant term since the sum of $\boldsymbol{u}$ is equal to MG at steady state.

Hence, the problem in Eq. Eq. 13 can be redefined as:

$$\min \boldsymbol{u}^{\mathrm{T}}\boldsymbol{u} \text{ subject to } P(\boldsymbol{\theta})\boldsymbol{u} = \boldsymbol{G} \tag{15}$$

When $N = 4$ and P is full rank, Eq. 12 can be solved as $\boldsymbol{u} = P^{-1}G$. However, for a system with more than four links, a null space occurs, resulting in an infinite solution for $\boldsymbol{u}$. In this case, we use Lagrange multiplier to obtain least-norm solution of $\boldsymbol{u}$ since the purpose is to minimize the norm of $\boldsymbol{u}$ as shown in Eq. 15.

The Lagrange multiplier can be written as:

$$\boldsymbol{u} = P(PP^{\mathrm{T}})^{-1}\boldsymbol{G} \tag{16}$$

B. Constraints of Form of Multilinks

Although the optimal form can be obtained as described in Eq. 15, the solution can be invalid. Therefore, the solution must satisfy constraints for avoidance of invalid forms. Five constraints are shown as follows.

1) Joint Angle Limit: In this work, the rotation range of each joint is $-\frac{\pi}{2}$[rad] $\sim \frac{\pi}{2}$[rad]. The joint angles must be changed in this range since a command of joint angle which is out of this range does not make sense.

2) Self-Collision: Although the joint angles are in the range, self-collision can occur as shown in Fig. 3(a). Therefore, collision detection is necessary to avoid self-collision.

3) Rank of P: According to Eq. 4, if P has full rank, the mapping is surjective, indicating that the four elements in $\boldsymbol{y}$ $(z, \varphi, \theta, \psi)$ are dependent of each other. In contrast, if P is not of full rank, the four elements can not act independently, leading to an uncontrollable result. We call the resulting special form the singular form(Fig. 3(b)).The rank of P can be calculated by checking the linear combination of row vectors $(\mathbf{p}_z, \mathbf{p}_x, \mathbf{p}_y, \mathbf{p}_c)$. It is evident that $\mathbf{p}_z$ and $\mathbf{p}_c$ are linearly independent, and the linear independence of the two group $(\{\mathbf{p}_z, \mathbf{p}_x, \mathbf{p}_y\}$ and $\{\mathbf{p}_c, \mathbf{p}_x, \mathbf{p}_y\})$ must be checked. When the multirotor is under the singular form, its control system is asymptotically unstable.

4) Lifting Force Range: Lifting force which is generated by the propeller has the range. In the case of our own machine, the range of lifting force is (0[N]$\sim$16.5[N]). All elements of the input vector $\boldsymbol{u}$ in Eq. 16 must fall within this range of forces.

5) Distance from Each Propeller to the Rotational Axis: There can be unavoidable errors in the control model(Eq. 4) and state equation(Eq. 5) because of estimation errors in the inertia parameters. The most serious error concerns the estimation of x_i and y_i as shown in Fig. 4. The distance x_i, y_i has a significant effect on the moment for pitch and roll rotation, especially when all elements in x or y are close to zero, in which case the estimation error can assign the wrong sign of x_i, y_i, producing a roll/pitch moment in the wrong direction.

To avoid this, it is necessary to keep the distance x_i, y_i large enough. We, therefore, introduce the following distance indices d_x, d_y to evaluate each state:

$$\begin{cases} d_x(State(\boldsymbol{\theta})) = \frac{\min(|\min(\boldsymbol{x}(\boldsymbol{\theta}))|, \max(\boldsymbol{x}(\boldsymbol{\theta})))}{r} \\ d_y(State(\boldsymbol{\theta})) = \frac{\min(|\min(\boldsymbol{y}(\boldsymbol{\theta}))|, \max(\boldsymbol{y}(\boldsymbol{\theta})))}{r} \end{cases} \tag{17}$$

We then use the indices to validate the state in terms of the distance of pitch/roll moment, using a thresholding method as follows:

$$Validator_{dist}(State(\boldsymbol{\theta})) =$$
$$\begin{cases} Valid & (d_x(State(\boldsymbol{\theta})) >= Threshold \\ & AND\ d_y(State(\boldsymbol{\theta})) >= Threshold) \\ Invalid & (d_x(State(\boldsymbol{\theta})) < Threshold \\ & OR\ d_y(State(\boldsymbol{\theta})) < Threshold) \end{cases} \tag{18}$$

The target state will be validated as an invalid state, if either of the two indices fall below the threshold. The form shown in Fig. 3(c) is an example of an invalid state.

C. Optimal Form Based on Gradient Descent

To determine the joint angle vector $\boldsymbol{\theta}$ which minimizes $\boldsymbol{u}^{\mathrm{T}}\boldsymbol{u}$(Eq. 15, Eq. 16), we apply gradient descent. In gradient
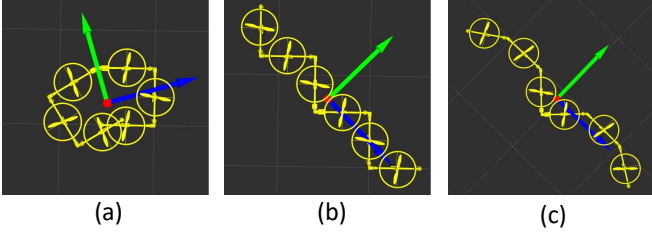
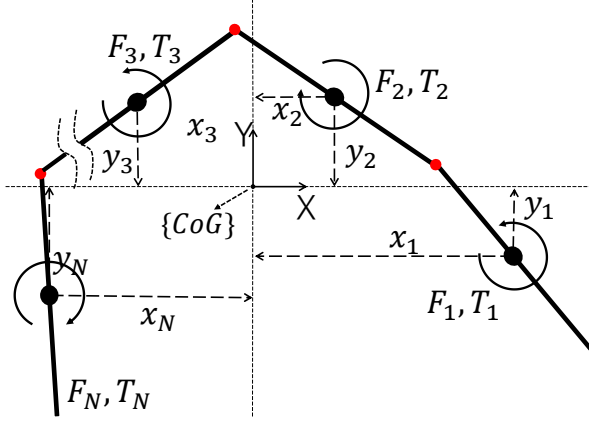(a)   (b)   (c)

Fig. 3.   Invalid forms.

Fig. 4.   The dynamic model of the quadrotor prototypetype described in coordinate frame $\{CoG\}$. F_i and T_i denote the lifting force and torque generated by each propeller, respectively. $[x_i, y_i]$ is the location of each propeller in the frame of $\{CoG\}$.

parameter	value	description
α	0.3	weight of update[rad^2/N^2]
m_{UAV}	5	UAV mass[kg]
m_{obj}	0.5	additional mass[kg]
V_{th}	0.001	lower limit of $V(\boldsymbol{u})$[N^2]

(a) $V(\boldsymbol{u})$: 0.000885   (b) $V(\boldsymbol{u})$: 0.000883

(c) $V(\boldsymbol{u})$: 0.000928   (d) $V(\boldsymbol{u})$: 0.000075
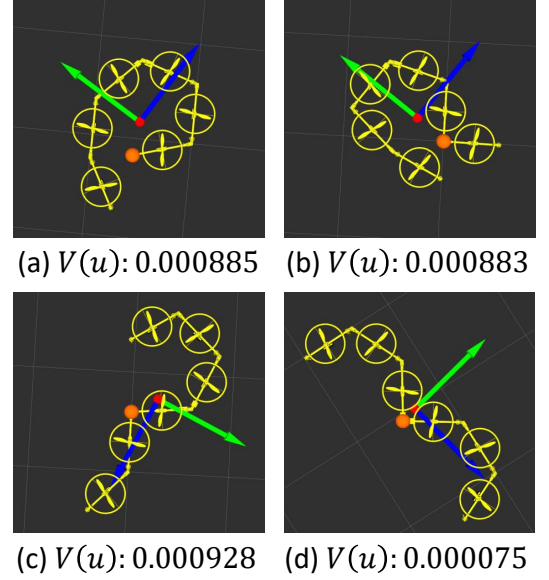
Fig. 5.   The optimized forms of each case with steepest descent.

descent, the joint angle vector $\boldsymbol{\theta}$ is updated as follows:

$$\boldsymbol{\theta}^{(k+1)} = \boldsymbol{\theta}^{(k)} - \alpha \ \mathrm{grad}(F(\boldsymbol{\theta}^{(k)})) \qquad (19)$$

$$F(\boldsymbol{\theta}) = \boldsymbol{u}(\boldsymbol{\theta})^{\mathrm{T}} \boldsymbol{u}(\boldsymbol{\theta})$$

Note that α is the parameter which determines the weight of one update and is normally defined as small positive value. Although F is necessary to be differentiable, it is a simple method since only first derivative must be caluclated. In this work, as it is difficult to calculate partial derivative of F, instead of this, we calculate variation of F. This is written as:

$$\mathrm{grad}(F(\boldsymbol{\theta}))_i = \frac{F(\boldsymbol{\theta} + \Delta\boldsymbol{\theta_i}) - F(\boldsymbol{\theta})}{\Delta\theta} \qquad (20)$$

where $\Delta\theta$ and $\Delta\boldsymbol{\theta_i}$ are infinitesimal angle and column vector whose i-th component is $\Delta\theta$ and the other components are 0, respectively. We also introduce V_{th}, the lower limit of $V(\boldsymbol{u})$ as a termination condition of optimization. Since the upper limit of lifting force is 16.5[N] in the case of our own machine, we set V_{th} to 0.001[N^2]. In other words, we stop the optimization when $V(\boldsymbol{u})$ is 0.001[N^2] since the value can be considered to be converged fully. Besides, since the solution obtained by gradient descent depends on the initial value, there is a possibility that valid solution is not obtained. Accordingly, we perform optimization with multiple initial values($\theta_i = 0.0, 0.1, \cdots, 1.0$).

Then, setting parameters of gradient descent as shown in Table I, we perform optimization calculation on four conditions shown in Fig. 5. In Fig. 5(a) $\sim$ Fig. 5(d), the orange circle indicates the position of the additional mass(0.5[kg]) while the red circle and the blue, green arrows indicate the position of CoG and principal axes of inertia, respectively. According to the final values of $V(\boldsymbol{u})$ shown under each form, it is evident that the optimization is fully performed and optimal forms can be obtained by this method.

V. HARDWARE AND SOFTWARE SYSTEM

A. Structure of Link Module

We constructed the link module of the multilink as shown in Fig. 6(a). Each link module has a build-in propeller at the center. A servo motor at the end of the link module comprised the main part of the joint module. The rotation range of each joint is $-\frac{\pi}{2}$[rad] $\sim$ $\frac{\pi}{2}$[rad]. The multilink can transform only in two-dimentions due to the joints with the same rotational axis. The range of lifting force is (0[N]$\sim$16.5[N]).

B. Structure of Electromagnet Gripper

In this work, limiting objects transported by the aerial robot to ferrous objects, we construct an electromagnet gripper(Fig. 6(b)). The gripper comprises five electromagnets whose diameter is 20[mm] and four micro switches. Contact with an object can be detected by the signal of micro
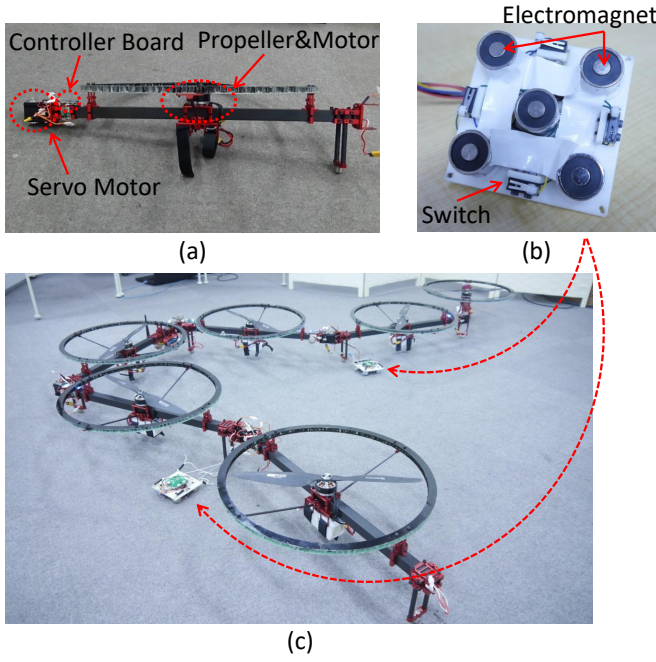
Fig. 6. Hardware.

Fig. 7. Internal communication.

(a) Neuron   (b) Spinal

Fig. 8. Controller board.

switches. The electromagnets are driven only while any switch is turned on to save the energy of batteries and to avoid the overheating of electromagnets. As shown in Fig. 6(c), the grippers are connected to the aerial robot with strings because the gripper can move passively at the time of contact to an object.

C. Multi-Layer Structure for Internal Communication

The multilink has not only motors for rotation of propeller but also servo motors for transform as actuator. Besides, the length of the multilink is longer than conventional aerial robots. In the conventional method, an aerial robot has only one central processor connected to all actuators and sensors. However, it is assumed that if we provide the conventional method for the multilink, the possibility of disconnection increases due to the length of the multilink.

For the reason noted above, we constructed multi-layer structure for internal communication(Fig. 7). As shown in Fig. 6(a), each link module has the controller board(Neuron)(Fig. 8(a)) which sends data to the motor and servo motor and receives data from IMU(Inertia Measurement Unit). Moreover, the center link has the other controller board(Spinal)(Fig. 8(b)) which communicates with each Neuron. We use CAN(Controller Area Network) to construct the communication system between the controller boards. As used in cars, CAN is a reliable communication system which resists external noise. Thereby, the amount of electric wiring descreases resulting that the reliability of the communication improves.

Moreover, the computer is connected to Spinal on USB-serial communication. The LQI control, motion planning, etc are executed on the computer.
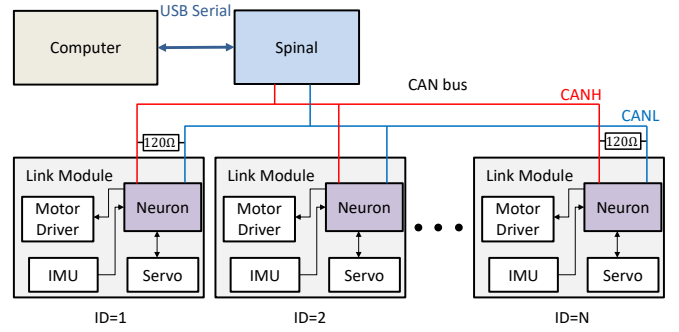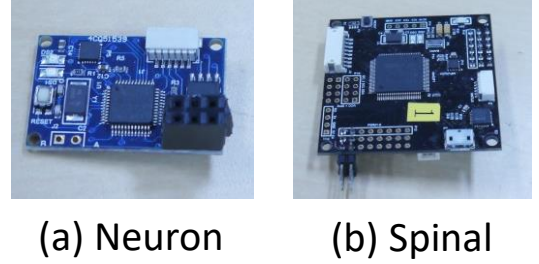
VI. EXPERIMENTS

VII. CONCLUSIONS

REFERENCES

[1] Vijay Kumar and Nathan Michael. Opportunities and challenges with autonomous micro aerial vehicles. *The International Journal of Robotics Research*, Vol. 31, No. 11, pp. 1279–1291, 2012.
[2] Quentin Lindsey, Daniel Mellinger, and Vijay Kumar. Construction with quadrotor teams. *Autonomous Robots*, Vol. 33, No. 3, pp. 323–336, 2012.
[3] Moju Zhao, Koji Kawasaki, Kei Okada, and Masayuki Inaba. Transformable multirotor with two-dimensional multilinks: modeling, control, and motion planning for aerial transformation. *Advanced Robotics*, Vol. 30, No. 13, pp. 825–845, 2016.
[4] *Whole-body Aerial Manipulation by Transformable Multirotor with Two-dimensional Multilinks*, 2017.
[5] P. C. YOUNG and J. C. WILLEMS. An approach to the linear multivariable servomechanism problem † . *International Journal of Control*, Vol. 15, No. 5, pp. 961–979, 1972.
[6] Moju Zhao, Koji Kawasaki, Yohei Kakiuchi, Kei Okada, and Masayuki Inaba. Simultaneous environment modeling and deployment of network by dropping wireless modules based on radio field intensity measurement using an micro aerial robot. *Journal of the Robotics Society of Japan*, Vol. 32, No. 7, pp. 643–650, 2014.